# A two-dimensional finite volume solution of dam-break hydraulics over erodible sediment beds

**Fayssal Benkhaldoun, Imad Elmahi, Saïda Sari, and Mohammed Seaïd**

**Abstract** Two-dimensional dam-break hydraulics over erodible sediment beds are solved using a well-balanced finite volume method. The governing equations consist of three coupled model components: (i) the shallow water equations for the hydrodynamical model, (ii) a transport equation for the dispersion of suspended sediments, and (iii) an Exner equation for the morphological model. These coupled models form a hyperbolic system of conservation laws with source terms. The proposed finite volume method consists of a predictor stage for the discretization of gradient terms and a corrector stage for the treatment of source terms. The gradient fluxes are discretized using a modified Roe's scheme using the sign of the Jacobian matrix in the coupled system. A well-balanced discretization is used for the treatment of source terms. In this paper, we also describe an adaptive procedure in the finite volume method by monitoring the concentration of suspended sediments in the computational domain during its transport process. The method uses unstructured meshes, incorporates upwinded numerical fluxes and slope limiters to provide sharp resolution of steep sediment concentration and bed-load gradients that may form in the approximate solution.

**Keywords** Sediment transport, shallow water equations, finite volume method
**MSC2010:** 35L65, 65L08, 65C20

Fayssal Benkhaldoun and Saïda Sari
LAGA, Université Paris 13, 99 Av J.B. Clement, 93430 Villetaneuse, France,
e-mail: fayssal@math.univ-paris13.fr, sari@math.univ-paris13.fr

Imad Elmahi
ENSAO Complex Universitaire, B.P. 669, 60000 Oujda, Morocco, e-mail: ielmahi@ensa.univ-oujda.ac.ma

Mohammed Seaïd
School of Engineering and Computing Sciences, University of Durham, South Road, Durham DH1 3LE, UK, e-mail: m.seaid@durham.ac.uk

J. Fořt et al. (eds.), *Finite Volumes for Complex Applications VI – Problems & Perspectives*, Springer Proceedings in Mathematics 4,
DOI 10.1007/978-3-642-20671-9_88, 

## 1 Introduction

The main concern of the sediment transport (or morphodynamics) is to determine the evolution of bed levels for hydrodynamics systems such as rivers, estuaries, bays and other nearshore regions where water flows interact with the bed geometry. Example of applications include among others, beach profile changes due to severe wave climates, seabed response to dredging procedures or imposed structures, and harbour siltation. The ability to design numerical methods able to predict the morphodynamics evolution of the coastal seabed has a clear mathematical and engineering relevances. In practice, morphodynamics involve coupling between a hydrodynamics model, which provides a description of the flow field leading to a specification of local sediment transport rates, and an equation for bed level change which expresses the conservative balance of sediment volume and its continual redistribution with time. Here, the hydrodynamic model is described by the shallow water equations, the bed-load is modelled by the Exner equation, and the suspended sediment transport is modelled by an advection equation accounting for erosion and deposition effects. The coupled models form a hyperbolic system of conservation laws with a source term. Nowadays, much effort has been devoted to develop numerical schemes for morphodynamics models able to resolve all hydrodynamics and morphodynamics scales. In the current study, a class of finite volume methods is proposed for numerical simulation of transient flows involving erosion and deposition of sediments. The method consists of a predictor stage where the numerical fluxes are constructed and a corrector stage to recover the conservation equations. The sign matrix of the Jacobian matrix is used in the reconstruction of the numerical fluxes. Most of these techniques have been recently investigated in [1,2] for solving sediment transport models without accounting for erosion and deposition effects. The current study presents an extension of this method to transient flows involving erosion and deposition of sediments. A detailed formulation of the sign matrix and the numerical fluxes is presented. The proposed method also satisfies the property of well-balancing flux-gradient and source-term in the system. Numerical results and comparisons will be shown for several suspended sediment transport problems.

## 2 The governing equations

In the current study, the sediment transport model consists of three parts: A hydraulic variables describing the motion of water, a concentration variable describing the dispersion of suspended sediments, and a morphology variable which describes the deformation of the bed-load. In the present work we assume that the flow is almost horizontal, the vertical component of the acceleration is vanishingly small, the pressure is taken to be hydrostatic, the free-surface gravity waves are long with respect to the mean flow depth and wave amplitude, and the

water-species mixture is vertically homogeneous and non-reactive. The governing equations are obtained by balancing the net inflow of mass, momentum and species through boundaries of a control volume during an infinitesimal time interval while accounting for the accumulation of mass, resultant forces and species within the control volume, compare for example [1, 17] among others. Thus, the equations for mass conservation and momentum flux balance are given by

$$\begin{aligned}
&\frac{\partial h}{\partial t}+\frac{\partial (hu)}{\partial x}+\frac{\partial (hv)}{\partial y}=\frac{E-D}{1-p},\\
&\frac{\partial (hu)}{\partial t}+\frac{\partial}{\partial x}\left(hu^2+\frac{1}{2}gh^2\right)+\frac{\partial}{\partial y}\left(huv\right)=gh\left(-\frac{\partial Z}{\partial x}-S_f^x\right)-\frac{(\rho_s-\rho_w)}{2\rho}gh^2\frac{\partial c}{\partial x}\\
&\qquad\qquad -\frac{(\rho_0-\rho)(E-D)}{\rho(1-p)}u, \qquad (1)\\
&\frac{\partial (hv)}{\partial t}+\frac{\partial}{\partial x}\left(huv\right)+\frac{\partial}{\partial y}\left(hv^2+\frac{1}{2}gh^2\right)=gh\left(-\frac{\partial Z}{\partial y}-S_f^y\right)-\frac{(\rho_s-\rho_w)}{2\rho}gh^2\frac{\partial c}{\partial y}\\
&\qquad\qquad -\frac{(\rho_0-\rho)(E-D)}{\rho(1-p)}v,
\end{aligned}$$

where $t$ is the time variable, $\mathbf{x}=(x,y)^T$ the space coordinates, $\mathbf{u}=(u,v)^T$ the depth-averaged water velocity, $h$ the water depth, $Z$ the bottom topography, $g$ the gravitational acceleration, $p$ the porosity, $\rho_w$ the water density, $\rho_s$ the sediment density, $c$ is the depth-averaged concentration of the suspended sediment, $E$ and $D$ represent the entrainment and deposition terms in upward and downward directions, respectively. In (1), $\rho$ and $\rho_0$ are respectively, the density of the water-sediment mixture and the density of the saturated bed defined by

$$\begin{aligned}
\rho&=\rho_w(1-c)+\rho_s c,\\
\rho_0&=\rho_w p+\rho_s(1-p).
\end{aligned} \qquad (2)$$

The friction slopes $S_f^x$ and $S_f^y$ are defined, using the Manning roughness coefficient $n_b$, as

$$S_f^x=\frac{n_b^2}{h^{4/3}}u\sqrt{u^2+v^2}, \qquad S_f^y=\frac{n_b^2}{h^{4/3}}v\sqrt{u^2+v^2}. \qquad (3)$$

The equation for mass conservation of species is modeled by

$$\frac{\partial (hc)}{\partial t}+\frac{\partial}{\partial x}\left(huc\right)+\frac{\partial}{\partial y}\left(hvc\right)=E-D. \qquad (4)$$

To determine the entrainment and deposition terms in the above equations we assume a non-cohesive sediment and we use empirical relations reported in [8]. Thus,

$$D = w(1 - C_a)^m C_a, \tag{5}$$

where $w$ is the settling velocity of a single particle in tranquil water

$$\omega = \frac{\sqrt{(36\nu/d)^2 + 7.5\rho_s g d} - 36\nu/d}{2.8}, \tag{6}$$

with $\nu$ is the kinematic viscosity of the water, $d$ the averaged diameter of the sediment particle, $m$ an exponent indicating the effects of hindered settling due to high sediment concentrations, $C_a$ the near-bed volumetric sediment concentration, $C_a = \alpha_c c$, where $\alpha_c$ is a coefficient larger than unity. To ensure that the near-bed concentration does not exceed $(1 - p)$, the coefficient $\alpha_c$ is computed by [10]

$$\alpha_c = \min\left(2, \frac{1-p}{c}\right).$$

For the entrainment of a cohesive material the following relation is used

$$E = \begin{cases} \varphi \dfrac{\theta - \theta_c}{h} \overline{u} d^{-0.2}, & \text{if } \theta \geq \theta_c, \\ 0, & \text{otherwise,} \end{cases} \tag{7}$$

where

$$\overline{u} = \sqrt{u^2 + v^2},$$

and $\varphi$ is a coefficient to control the erosion forces, $\theta_c$ is a critical value of Shields parameter for the initiation of sediment motion and $\theta$ is the Shields coefficient defined by

$$\theta = \frac{u_*^2}{sgd}, \tag{8}$$

with $u_*$ is the friction velocity defined using the Darcy-Weisbach friction factor $f$ as

$$u_*^2 = \sqrt{\frac{f}{8}} \overline{u}.$$

In (8), $s$ is the submerged specific gravity of sediment given by

$$s = \frac{\rho_s}{\rho_w} - 1.$$

To update the bedload, we consider the Exner equation proposed in [14]

$$\frac{\partial Z}{\partial t} + \frac{A_s}{1-p}\frac{\partial}{\partial x}\left(u(u^2+v^2)\right) + \frac{A_s}{1-p}\frac{\partial}{\partial y}\left(v(u^2+v^2)\right) = -\frac{E-D}{1-p}, \tag{9}$$

where $A_s$ is a coefficient usually obtained from experiments taking into account the grain diameter and the kinematic viscosity of the sediments. For simplicity in the presentation, let us rewrite the equations (1), (4) and (9) in the following vector form

$$\frac{\partial \mathbf{W}}{\partial t} + \frac{\partial \mathbf{F}(\mathbf{W})}{\partial x} + \frac{\partial \mathbf{G}(\mathbf{W})}{\partial y} = \mathbf{S}(\mathbf{W}) + \mathbf{Q}(\mathbf{W}), \tag{10}$$

where $\mathbf{W}$ is the vector of conserved variables, $\mathbf{F}$ and $\mathbf{G}$ are the physical fluxes in $x$- and $y$-direction, $\mathbf{S}$ and $\mathbf{Q}$ are the source terms. These variables are defined as

$$\mathbf{W} = \begin{pmatrix} h \\ hu \\ hv \\ hc \\ Z \end{pmatrix}, \quad \mathbf{F}(\mathbf{W}) = \begin{pmatrix} hu \\ hu^2 + \frac{1}{2}gh^2 \\ huv \\ huc \\ \frac{A_s}{1-p}u(u^2+v^2) \end{pmatrix}, \quad \mathbf{G}(\mathbf{W}) = \begin{pmatrix} hv \\ huv \\ hv^2 + \frac{1}{2}gh^2 \\ hvc \\ \frac{A_s}{1-p}v(u^2+v^2) \end{pmatrix},$$

$$\mathbf{S} = \begin{pmatrix} 0 \\ -gh\frac{\partial Z}{\partial x} - \frac{(\rho_s-\rho_w)}{2\rho}gh^2\frac{\partial c}{\partial x} \\ -gh\frac{\partial Z}{\partial y} - \frac{(\rho_s-\rho_w)}{2\rho}gh^2\frac{\partial c}{\partial y} \\ 0 \\ 0 \end{pmatrix}, \quad \mathbf{Q} = \begin{pmatrix} \frac{E-D}{1-p} \\ -ghS_f^x - \frac{(\rho_0-\rho)(E-D)}{\rho(1-p)}u \\ -ghS_f^y - \frac{(\rho_0-\rho)(E-D)}{\rho(1-p)}v \\ E-D \\ -\frac{E-D}{1-p} \end{pmatrix}.$$

It is worth emphasizing that, using the Exner equation (9) to model the bed-load transport, the nonhomegenuous terms in the right-hand side in (10) are not standard source terms but nonconservative products, since they include derivatives of two of the variables. The presence of these terms in sediment transport system can cause sever difficulties in their numerical approximations. In principle, the nonhomegenuous term in these equations can be viewed as a source term and/or a nonconservative term. In the approach presented in this study these terms are considered and discretized as source terms.

## 3 The finite volume method

The governing sediment transport equations (10) are formulated in Cartesian coordinates and will be discretized into the unstructured grids by the finite volume method. The unstructured grids are polygons and the number of edges of the grids is not limited in theory, but only triangular grids are considered in the current study. Hence, we divide the time interval into sub-intervals $[t_n, t_{n+1}]$ with stepsize $\Delta t$ and discretize the spatial domain in conforming triangular elements $\mathscr{T}_i$. Each triangle represents a control volume and the variables are located at the geometric centres of the cells. Hence, using the control volume depicted in Fig. 1, a finite volume discretization of (10) yields

$$\mathbf{W}_i^{n+1} = \mathbf{W}_i^n - \frac{\Delta t}{|\mathscr{T}_i|} \sum_{j \in N(i)} \int_{\Gamma_{ij}} \mathscr{F}(\mathbf{W}^n; \mathbf{n})\, d\sigma + \frac{\Delta t}{|\mathscr{T}_i|} \int_{\mathscr{T}_i} \mathbf{S}(\mathbf{W}^n)\, dV + \frac{\Delta t}{|\mathscr{T}_i|} \int_{\mathscr{T}_i} \mathbf{Q}(\mathbf{W}^n)\, dV, \tag{11}$$

where $N(i)$ is the set of neighboring triangles of the cell $\mathscr{T}_i$, $\mathbf{W}_i^n$ is an averaged value of the solution $\mathbf{W}$ in the cell $\mathscr{T}_i$ at time $t_n$,

$$\mathbf{W}_i = \frac{1}{|\mathscr{T}_i|} \int_{\mathscr{T}_i} \mathbf{W}\, dV,$$

where $|\mathscr{T}_i|$ denotes the area of $\mathscr{T}_i$ and $\mathscr{S}_i$ is the surface surrounding the control volume $\mathscr{T}_i$. Here, $\Gamma_{ij}$ is the interface between the two control volumes $\mathscr{T}_i$ and $\mathscr{T}_j$, $\mathbf{n} = (n_x, n_y)^T$ denotes the unit outward normal to the surface $\mathscr{S}_i$, and

$$\mathscr{F}(\mathbf{W}; \mathbf{n}) = \mathbf{F}(\mathbf{W}) n_x + \mathbf{G}(\mathbf{W}) n_y.$$

To deal with the source terms $\mathbf{Q}$, a standard splitting procedure (see for instance [2]) is employed for the discrete system (11) as

$$\begin{aligned} \mathbf{W}_i^* &= \mathbf{W}_i^n - \frac{\Delta t}{|\mathscr{T}_i|} \sum_{j \in N(i)} \int_{\Gamma_{ij}} \mathscr{F}(\mathbf{W}^n; \mathbf{n})\, d\sigma + \frac{\Delta t}{|\mathscr{T}_i|} \int_{\mathscr{T}_i} \mathbf{S}(\mathbf{W}^n)\, dV, \\ \mathbf{W}_i^{n+1} &= \mathbf{W}_i^* + \frac{\Delta t}{|\mathscr{T}_i|} \int_{\mathscr{T}_i} \mathbf{Q}(\mathbf{W}^*)\, dV. \end{aligned} \tag{12}$$

Note that the time splitting (12) is only first-order accurate. A second-order splitting for the system (11) can be derived analogously using the Strang method [16]. The finite volume discretization (11) is complete once the gradient fluxes $\mathscr{F}(\mathbf{W}; \mathbf{n})$ and a discretization of source terms $\mathbf{Q}(\mathbf{W}^n)$ and $\mathbf{S}(\mathbf{W}^n)$ are well defined.

For the discretization of the gradient fluxes we consider a modified Roe's method studied in [3–6] among others. The method consists of the predictor-corrector

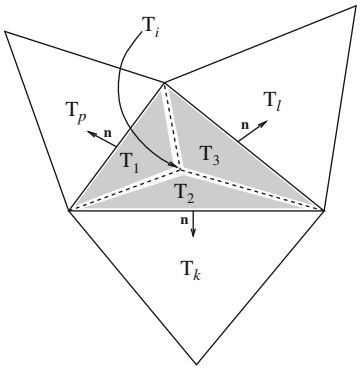


**Fig. 1** A generic control volume $\mathscr{T}_i$ and notations

procedure

$$\begin{aligned}\mathbf{U}_{ij}^{n} &= \frac{1}{2}\left(\mathbf{U}_{i}^{n}+\mathbf{U}_{j}^{n}\right)-\frac{1}{2}\,\mathrm{sgn}\Big[\mathbf{A}_{\eta}\left(\overline{\mathbf{U}}\right)\Big]\left(\mathbf{U}_{j}^{n}-\mathbf{U}_{i}^{n}\right),\\ \mathbf{W}_{i}^{n+1} &= \mathbf{W}_{i}^{n}-\frac{\Delta t}{|\mathscr{T}_i|}\sum_{j\in N(i)}\mathscr{F}\left(\mathbf{W}_{ij}^{n};\eta_{ij}\right)|\Gamma_{ij}|+\Delta t\mathbf{S}_{i}^{n},\end{aligned} \tag{13}$$

where

$$\mathbf{U}=\begin{pmatrix}h\\ u_\eta\\ u_\tau\\ c\\ Z\end{pmatrix},\quad \mathbf{A}_\eta(\mathbf{U})=\begin{pmatrix}u_\eta & h & 0 & 0 & 0\\ g & u_\eta & 0 & \dfrac{(\rho_s-\rho_w)}{2\rho}gh & g\\ 0 & 0 & u_\eta & 0 & 0\\ 0 & 0 & 0 & u_\eta & 0\\ 0 & \dfrac{A_s}{1-p}(3\,u_\eta^2+u_\tau^2) & 2\dfrac{A_s}{1-p}u_\eta\,u_\tau & 0 & 0\end{pmatrix}.$$

the normal velocity $u_\eta = un_x + vn_y$ and tangential velocity $u_\tau = un_y - vn_x$. The sign matrix of the Jacobian is defined as

$$\mathrm{sgn}\Big[\nabla\mathbf{F}_\eta\left(\overline{\mathbf{U}}\right)\Big]=\mathscr{R}(\overline{\mathbf{U}})\,\mathrm{sgn}\Big[\Lambda(\overline{\mathbf{U}})\Big]\mathscr{R}^{-1}(\overline{\mathbf{U}}),$$

with $\Lambda(\overline{\mathbf{U}})$ is the diagonal matrix of eigenvalues, and $\mathscr{R}(\overline{\mathbf{U}})$ is the right eigenvector matrix. These matrices can be explicitly expressed using the associated eingenvalues of $\mathbf{A}_\eta(\mathbf{U})$. The sign matrix can be formulated in the same manner as in [3–6] and details are omitted here. In (13), $\overline{\mathbf{U}}$ is the Roe's average state given by

$$\overline{\mathbf{U}} = \begin{pmatrix} \dfrac{h_i + h_j}{2} \\ \dfrac{u_i\sqrt{h_i} + u_j\sqrt{h_j}}{\sqrt{h_i} + \sqrt{h_j}}\eta_x + \dfrac{v_i\sqrt{h_i} + v_j\sqrt{h_j}}{\sqrt{h_i} + \sqrt{h_j}}\eta_y \\ -\dfrac{u_i\sqrt{h_i} + u_j\sqrt{h_j}}{\sqrt{h_i} + \sqrt{h_j}}\eta_y + \dfrac{v_i\sqrt{h_i} + v_j\sqrt{h_j}}{\sqrt{h_i} + \sqrt{h_j}}\eta_x \\ \dfrac{c_i\sqrt{h_i} + c_j\sqrt{h_j}}{\sqrt{h_i} + \sqrt{h_j}} \\ \dfrac{Z_i + Z_j}{2} \end{pmatrix}. \tag{14}$$

Next we discuss the treatment of source terms $\mathbf{S}_i^n$ in the proposed finite volume scheme and also the extension of the scheme to a second-order accuracy. An adaptive procedure is also described in this section.

### *3.1 Treatment of the source term*

The treatment of the source terms in the shallow water equations presents a challenge in many numerical methods. In our scheme, the source term approximation $\mathbf{S}_i^n$ in the corrector stage is reconstructed such that the still-water equilibrium (C-property) is satisfied. Here, a numerical scheme is said to satisfy the C-property for the equations (10) if the condition

$$E - D = 0, \qquad u = 0, \qquad Z = \bar{Z}(x), \qquad h + Z = H, \qquad \rho = C, \tag{15}$$

holds for stationary flows at rest. In (15), $H$ and $C$ are nonnegative constants. Therefore, the treatment of source terms in (13) is reconstructed such that the condition (15) is preserved at the discretized level. Remark that the last condition in (15) means that at the equilibrium the sediment medium is assumed to be saturated. Furthermore, from the density equation (2), a constant density is equivalent to a constant concentration $c$. Hence, $\mathbf{S}_i^n$ should be consistent discretization of the source term in (13) defined as

$$\mathbf{S}_i^n = \begin{pmatrix} 0 \\ -g\bar{h}_{xi}^n \displaystyle\sum_{j\in N(i)} Z_{ij} n_{xij} \left|\Gamma_{ij}\right| - \dfrac{(\rho_s - \rho_w)}{2\rho} g \left(\bar{h}_{xi}^n\right)^2 \displaystyle\sum_{j\in N(i)} c_{ij} n_{xij} \left|\Gamma_{ij}\right| \\ -g\bar{h}_{yi}^n \displaystyle\sum_{j\in N(i)} Z_{ij} n_{yij} \left|\Gamma_{ij}\right| - \dfrac{(\rho_s - \rho_w)}{2\rho} g \left(\bar{h}_{yi}^n\right)^2 \displaystyle\sum_{j\in N(i)} c_{ij} n_{yij} \left|\Gamma_{ij}\right| \\ 0 \\ 0 \end{pmatrix}. \tag{16}$$

The approximations $\bar{h}^n_{xi}$ and $\bar{h}^n_{yi}$ are reconstructed using a technique recently developed in [3] for the proposed finite volume method to satisfy the well-known C-property. In this section we briefly describe the formulation of this procedure and more details can be found in [3]. Hence, at the stationary state, the numerical flux in the corrector stage yields

$$\sum_{j\in N(i)} \mathscr{F}\left(\mathbf{W}^n_{ij};\mathbf{n}_{ij}\right) = \begin{pmatrix} 0 \\ -g\int_{T_i} h\frac{\partial Z}{\partial x}\,dV - g\frac{(\rho_s-\rho_w)}{2\rho}\int_{T_i} h^2\frac{\partial c}{\partial x}\,dV \\ -g\int_{T_i} h\frac{\partial Z}{\partial y}\,dV - g\frac{(\rho_s-\rho_w)}{2\rho}\int_{T_i} h^2\frac{\partial c}{\partial y}\,dV \\ 0 \\ 0 \end{pmatrix},$$

which is equivalent to

$$\begin{pmatrix} 0 \\ \sum_{j\in N(i)} \frac{1}{2}g\left(h^n_{ij}\right)^2 N_{xij} \\ \sum_{j\in N(i)} \frac{1}{2}g\left(h^n_{ij}\right)^2 N_{yij} \\ 0 \\ 0 \end{pmatrix} = \begin{pmatrix} 0 \\ -g\int_{T_i} h\frac{\partial Z}{\partial x}\,dV - g\frac{(\rho_s-\rho_w)}{2\rho}\int_{T_i} h^2\frac{\partial c}{\partial x}\,dV \\ -g\int_{T_i} h\frac{\partial Z}{\partial y}\,dV - g\frac{(\rho_s-\rho_w)}{2\rho}\int_{T_i} h^2\frac{\partial c}{\partial y}\,dV \\ 0 \\ 0 \end{pmatrix}. \tag{17}$$

where $N_{xij} = n_{xij}\left|\Gamma_{ij}\right|$ and $N_{yij} = n_{yij}\left|\Gamma_{ij}\right|$. Next, to approximate the source terms we proceed as follows. First we decompose the triangle $T_i$ into three sub-triangles as depicted in Fig. 1. Then, the source term is approximated as

$$\int_{T_i} h\frac{\partial Z}{\partial x}\,dV = \int_{T_1} h\frac{\partial Z}{\partial x}\,dV + \int_{T_2} h\frac{\partial Z}{\partial x}\,dV + \int_{T_3} h\frac{\partial Z}{\partial x}\,dV, \tag{18}$$

where

$$\int_{T_1} h\frac{\partial Z}{\partial x}\,dV = h_1\int_{T_1}\frac{\partial Z}{\partial x}\,dV,$$

with $h_1$ is an average value of $h$ on the sub-triangle $T_1$. Hence,

$$\int_{T_1} h\frac{\partial Z}{\partial x}\,dV = h_1 \sum_{j\in N(1)} \int_{\Gamma_{1j}} Z n_x\,d\sigma,$$
$$= h_1 \sum_{j\in N(1)} Z_{1j}\ N_{x1j},$$
$$= h_1 \sum_{j\in N(1)} \frac{Z_1+Z_j}{2}\ N_{x1j}. \tag{19}$$

Again, using the stationary flow condition $h_1 + Z_1 = h_j + Z_j = H = constant$, one gets

$$h_1 + Z_1 + h_j + Z_j = 2H \qquad \text{and} \qquad \frac{Z_1+Z_j}{2} = H - \frac{h_1+h_j}{2}.$$

Thus, (19) gives

$$\int_{T_1} h\frac{\partial Z}{\partial x}\,dV = h_1 \sum_{j\in N(1)} \left(H - \frac{h_1+h_j}{2}\right) N_{x1j}.$$

Using the fact that $\sum_{j\in N(1)} N_{x1j} = 0$,

$$\int_{T_1} h\frac{\partial Z}{\partial x}\,dV = -\frac{h_1}{2} \sum_{j\in N(1)} h_j\ N_{x1j},$$
$$= -\frac{h_1}{2}\left(h_p N_{x1p} + h_2 N_{x12} + h_3 N_{x13}\right).$$

A similar procedure leads to the following approximations of the other terms in (18)

$$\int_{T_2} h\frac{\partial Z}{\partial x}\,dV = -\frac{h_2}{2}\left(h_k N_{x2k} + h_1 N_{x21} + h_3 N_{x23}\right),$$
$$\int_{T_3} h\frac{\partial Z}{\partial x}\,dV = -\frac{h_3}{2}\left(h_l N_{x3l} + h_1 N_{x31} + h_2 N_{x32}\right).$$

Notice that $h_p$, $h_k$ and $h_l$ are the average values of $h$ respectively, on the triangle $T_p$, $T_k$ and $T_l$, see Fig. 1. Summing up, the discretization (18) gives

$$\int_{T_i} h\frac{\partial Z}{\partial x}\,dV = -\frac{h_1}{2}h_p N_{x1p} - \frac{h_2}{2}h_k N_{x2k} - \frac{h_3}{2}h_l N_{x3l}.$$

For this reconstruction, the source terms in (16) result in

$$\begin{aligned}\sum_{j\in N(i)}\left(h_{ij}^{n}\right)^{2}N_{xij} &= h_1\left(h_pN_{x1p}\right)+h_2\left(h_kN_{x2k}\right)+h_3\left(h_lN_{x3l}\right),\\ \sum_{j\in N(i)}\left(h_{ij}^{n}\right)^{2}N_{yij} &= h_1\left(h_pN_{y1p}\right)+h_2\left(h_kN_{y2k}\right)+h_3\left(h_lN_{y3l}\right).\end{aligned} \tag{20}$$

Here, (20) forms a linear system of two equations for the three unknowns $h_1$, $h_2$ and $h_3$. To complete the system we add the natural conservation equation

$$h_1+h_2+h_3=3h_i.$$

Analogously, the bottom values $Z_j$, $j=1,2,3$ are reconstructed in each sub-triangle of $T_i$ as

$$Z_j+h_j^n=Z_i+h_i^n,\qquad j=1,2,3.$$

Finally, the source terms in (18) are approximated as

$$\begin{aligned}h_1\int_{T_1}\frac{\partial Z}{\partial x}\,dV &= h_1\left(\frac{Z_1+Z_p}{2}N_{x1p}+\frac{Z_1+Z_2}{2}N_{x12}+\frac{Z_1+Z_3}{2}N_{x13}\right),\\ h_2\int_{T_1}\frac{\partial Z}{\partial x}\,dV &= h_2\left(\frac{Z_2+Z_k}{2}N_{x2k}+\frac{Z_2+Z_1}{2}N_{x21}+\frac{Z_2+Z_3}{2}N_{x23}\right),\\ h_3\int_{T_1}\frac{\partial Z}{\partial x}\,dV &= h_3\left(\frac{Z_3+Z_l}{2}N_{x3l}+\frac{Z_3+Z_1}{2}N_{x31}+\frac{Z_3+Z_2}{2}N_{x32}\right),\end{aligned} \tag{21}$$

with a similar equation for the other source terms in the $y$-direction.

## 4 Numerical results

We present numerical results for a test problem of partial dam-break over erodible bed. In all the computations reported herein, the Courant number $Cr$ is set to 0.8 and the time stepsize $\Delta t$ is adjusted at each step according to the stability condition

$$\Delta t=Cr\min_{\Gamma_{ij}}\left(\frac{|T_i|+|T_j|}{2\left|\Gamma_{ij}\right|\max_p\left|(\lambda_p)_{ij}\right|}\right),$$

where $\Gamma_{ij}$ is the edge between two triangles $T_i$ and $T_j$. The water density $\rho_w=1000\,kg/m^3$ and the gravitational acceleration is fixed to $g=9.81\,m/s^2$.

We consider a 200 $m$ long and 200 $m$ wide flat reservoir with two different constant levels of water separated by a dam. At $t=0$ part of the dam breaks instantaneously. The dam is 10 $m$ thick and the breach is assumed to be 75 $m$ wide, as shown in Fig. 2. Initially, $u(x,y,0)=v(x,y,0)=0\,m/s$

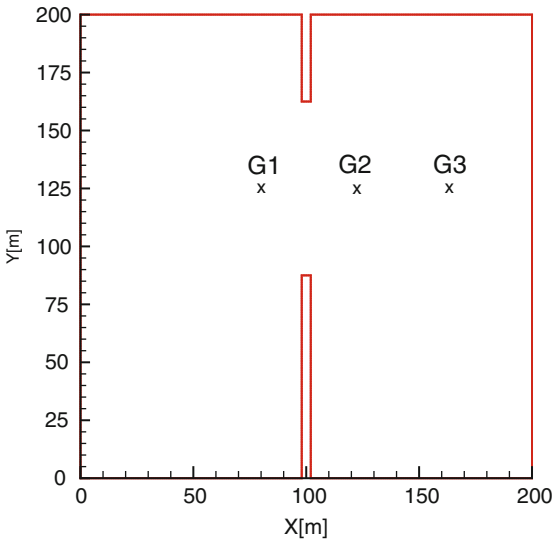


**Fig. 2** Computational domain for the partial dam-break over erodible bed

$$h(x,y,0) = \begin{cases} 10\,m, & \text{if} \quad x < 100\,m, \\ 1\,m, & \text{otherwise,} \end{cases} \qquad c(x,y,0) = \begin{cases} 0.01, & \text{if} \quad x < 100\,m, \\ 0, & \text{otherwise.} \end{cases}$$

The selected values for the evaluation of the present finite volume model are summarized in Table 1. At $t = 0$ the dam collapses and the flow problem consists of a shock wave traveling downstream and a rarefaction wave traveling upstream.

**Table 1** Reference parameters used for the dam-break problem

| Quantity | Reference value | Quantity | Reference value |
|---|---|---|---|
| $\rho_s$ | $1500\ kg/m^3$ | $\nu$ | $1.2 \times 10^{-6}\ m^2/s$ |
| $p$ | 0.28 | $n_b$ | $0.015\ s/m^{1/3}$ |
| $\varphi$ | $0.015\ m^{1.2}$ | $\theta_c$ | 0.045 |
| $m$ | 2 | $d$ | $1\ mm$ |

In Fig. 3 we present the water free-surface and bed-load, the adapted meshes and snapshots of the water depth obtained for the partial dam-break over fixed bed at times $t = 2$, 4, 6 and 8 $s$. The results obtained for the partial dam-break over erodible bed are presented in Fig. 4. By using adaptive meshes, high resolution is automatically obtained in those regions where the gradients of the water depth are steep such as the moving fronts. Apparently, the overall flow pattern for this

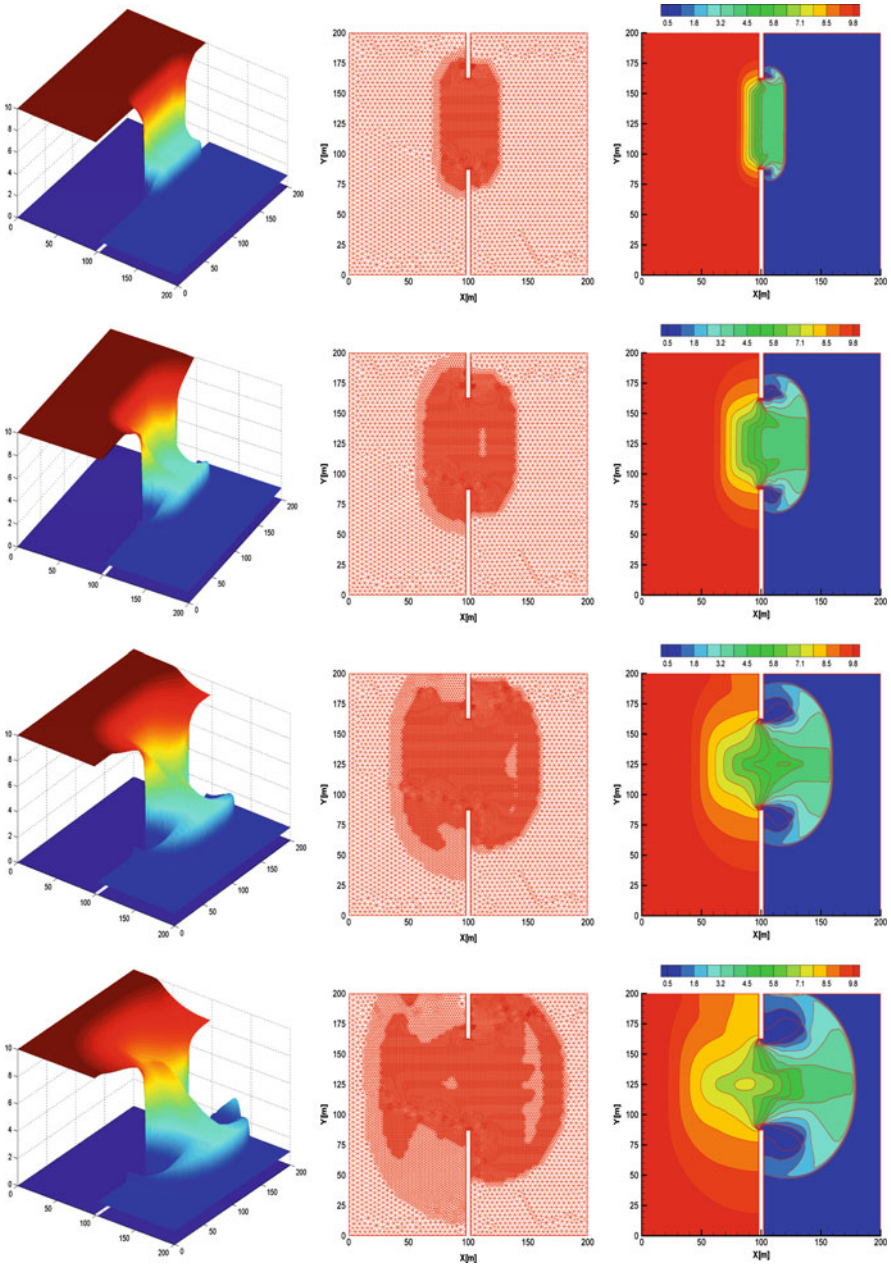


**Fig. 3** Water free-surface and bed-load (first column), adapted meshes (second column) and water free-surface contours (third column) for the partial dam-break over fixed bed at different simulation times. From top to bottom $t = 2$, 4, 6 and 8 $s$

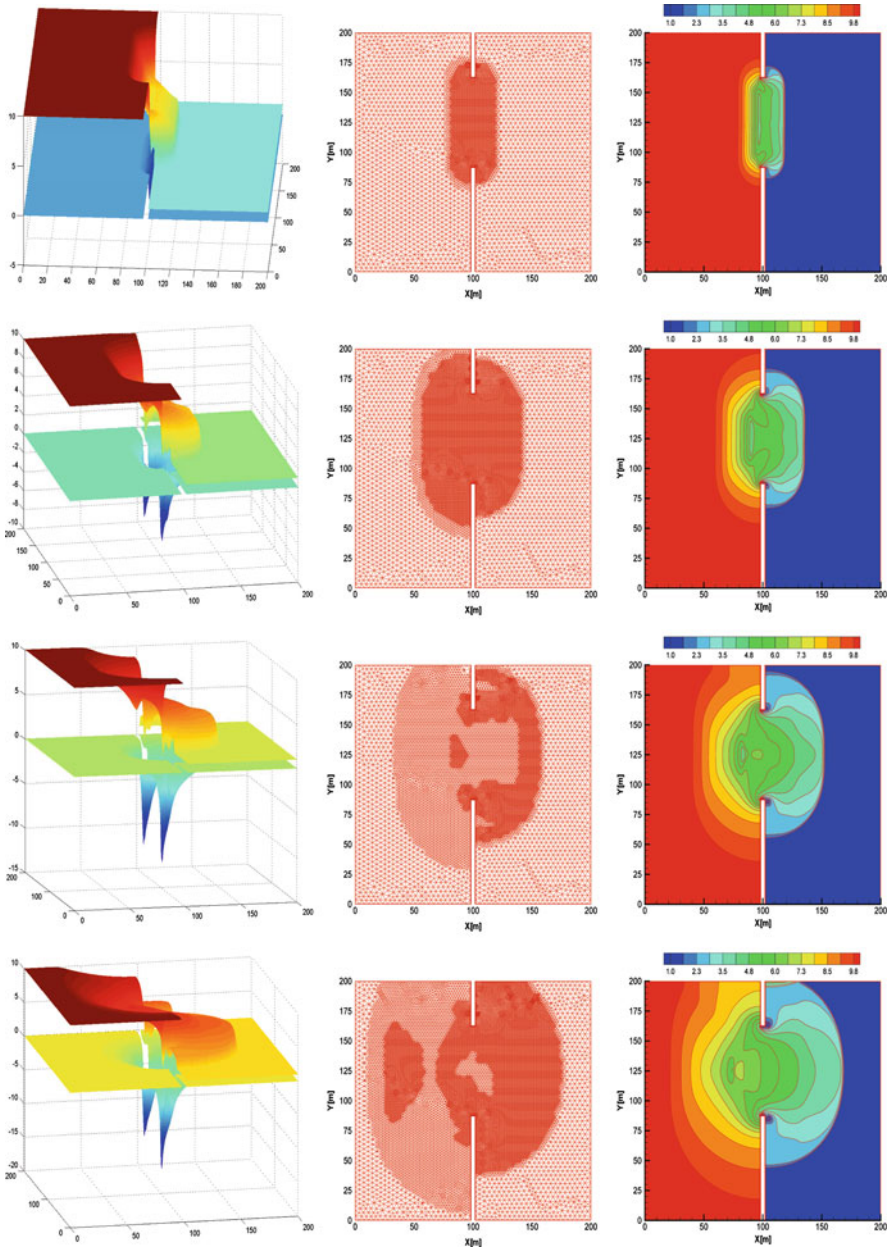


**Fig. 4** Water free-surface and bed-load (first column), adapted meshes (second column) and water free-surface contours (third column) for the partial dambreak over erodible bed at different simulation times. From top to bottom $t = 2$, 4, 6 and 8 $s$

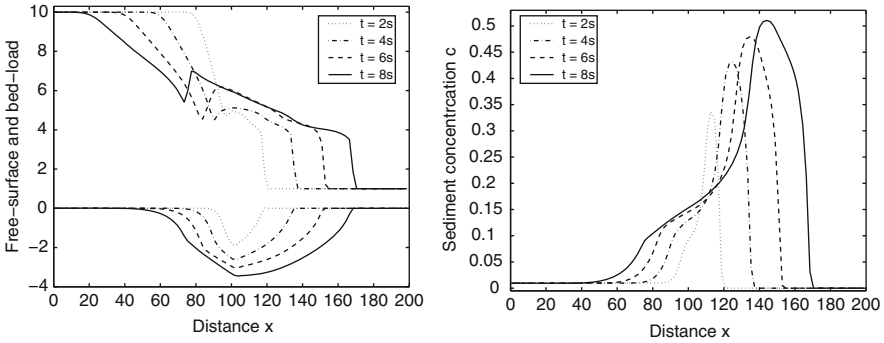


**Fig. 5** Cross sections at $y = 125\ m$ of the water free-surface and bed-load (left plot) and sediment concentration (right plot) at four instants

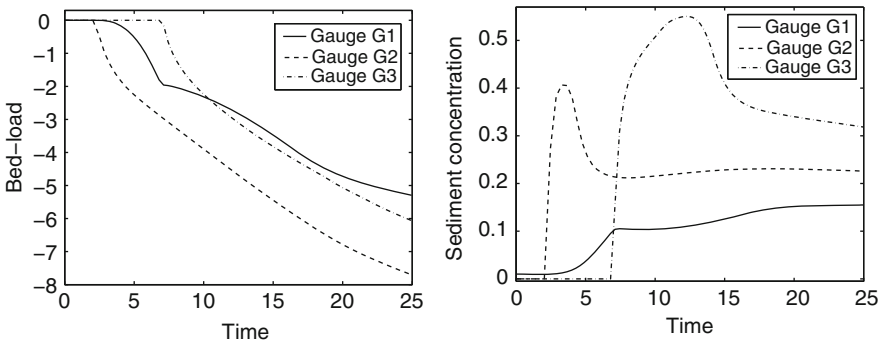


**Fig. 6** Time evolution of the water free-surface and bed-load (left plot) and sediment concentration (right plot) at the three gauges G1, G2 and G3 presented in Fig. 2

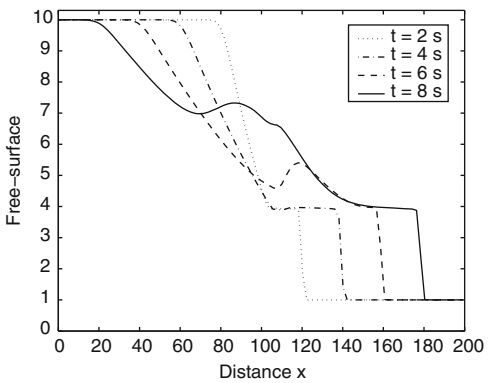


**Fig. 7** Cross sections at $y = 125\ m$ of the water free-surface for the partial dam-break over fixed bed

example is preserved with no excessive numerical diffusion in the results by finite volume method using adaptive mesh. The adaptive finite volume method performs well for this test problem since it does not diffuse the moving fronts and no spurious oscillations have been observed when the water flows over the movable bed.

In order to quantify the results for this test example we display in Fig. 5 cross sections at $y = 125\ m$ of the water free-surface and bed-load and sediment concentration at four instants shown in Fig. 4. The results for the partial dam-break over fixed bed are depicted in Fig. 7. Figure 6 exhibites the time evolution of the water free-surface, bed-load and sediment concentration at the three gauges G1, G2 and G3 presented in Fig. 2. As can be observed from these results, the erosion effects on the bed are clearly visible for the considered sediment conditions. The inclusion of Exner equation in the model creates a very active sediment exchange between the water flow and the bed load, and also produces a sharp spatial gradient of sediment concentration, which justifies its incorporation in the momentum equations (10). Apparently, the overall flow and sediment features for this example are preserved with no spurious oscillations appearing in the results obtained using the adaptive finite volume method. Obviously, the computed results verify the stability and the shock capturing properties of the proposed finite volume method.

## References


1. M.B. Abbott, Computational hydraulics: Elements of the theory of free surface flows, Fearon-Pitman Publishers, London, 1979.
2. S.J. Billett, E.F. Toro, On WAF-Type Schemes for Multidimensional Hyperbolic Conservation Laws, J. Comp. Physics. **130**, 1–24 (1997).
3. F. Benkhaldoun, I. Elmahi, M. Seaïd, "A new finite volume method for flux-gradient and source-term balancing in shallow water equations", Computer Methods in Applied Mechanics and Engineering. **199** pp:49-52 (2010).
4. F. Benkhaldoun, S. Sahmim, M. Seaïd, A two-dimensional finite volume morphodynamic model on unstructured triangular grids. Int. J. Num. Meth. Fluids. 63 (2010) 1296–1327.
5. F. Benkhaldoun, S. Sahmim, M. Seaïd, Solution of the sediment transport equations using a finite volume method based on sign matrix. SIAM J. Sci. Comp. 31 (2009) 2866–2889.
6. F. Benkhaldoun, I. Elmahi, M. Seaïd, "Well-balanced finite volume schemes for pollutant transport by shallow water equations on unstructured meshes", J. Comp. Physics. **226** pp:180-203 (2007).
7. K. Bloundi and J. Duplay, Heavy metals distribution in sediments of nador lagoon (Morocco), *Geophysical Research Abstracts*, **5**, pp. 11744, 2003.
8. Z. Cao and P. Carling. Mathematical modelling of alluvial rivers: reality and myth. Part I: General overview. Water Maritime Engineering. **154**, 207-220 (2002)
9. Z. Cao and G. Pender. Numerical modelling of alluvial rivers subject to interactive sediment mining and feeding. Advances in Water Resources. **27**, 533-546 (2004)
10. Z. Cao, G. Pender, S. Wallis and P. Carling. Computational dam-break hydraulics over erodible sediment bed. J. Hydraulic Engineering. **67**, 689-703 (2004)
11. Z. Cao, G. Pender and P. Carling. Shallow water hydrodynamic models for hyperconcentrated sediment-laden floods over erodible bed. Advances in Water Resources. **29**, 546-557 (2006)
12. N.S. Cheng, Simplified settling velocity formula for sediment paticle. J. Hydraulic Engineering ASCE. 123 (1997) 149–152.

13. J. Fredsøe, R. Deigaard, Mechanics of Coastal Sediment Transport. *Advanced Series on Ocean Engineering - Vol. 3*, 1992.
14. A.J. Grass, Sediment Transport by Waves and Currents. (SERC London Cent. Mar. Technol. Report No: FL29, 1981).
15. G. Simpson and S. Castelltort. Coupled model of surface water flow, sediment transport and morphological evolution. Computers & Geosciences. **32**, 1600-1614 (2006)
16. G. Strang. On the Construction and the Comparison of Difference Schemes. SIAM J. Numer. Anal. **5**, 506517 (1968)
17. C.Y. Yang,: Sediment Transport: Theory and Practice. McGraw-Hill, New York (1996)
18. R.L. Soulsby: Dynamics of marine sands, a manual for practical applications. HR Wallingford, Report SR 466 (1997)

The paper is in final form and no similar paper has been or is being submitted elsewhere.